




The Evolution of the Supersoft X-Ray Source WX Cen Dominated by Magnetic Wind

Lei Zang^{1,2,3} , Shengbang Qian^{1,2,3,4}, and Eduardo Fernández-Lajús^{5,6}¹ Yunnan Observatories, Chinese Academy of Sciences (CAS), P.O. Box 110, Kunming 650011, Yunnan, People's Republic of China; qsb@ynao.ac.cn² Key Laboratory of the Structure and Evolution of Celestial Objects, Chinese Academy of Sciences, P.O. Box 110, Kunming 650011, Yunnan, People's Republic of China³ University of Chinese Academy of Sciences, Yuquan Road 19#, Shijingshan District 100049, Beijing, People's Republic of China⁴ Center for Astronomical Mega-Science, Chinese Academy of Sciences, 20A Datun Road, Chaoyang District 100012, Beijing, People's Republic of China⁵ Facultad de Ciencias Astronómicas y Geofísicas—Universidad Nacional de La Plata, Paseo del Bosque S/N—B1900FWA, La Plata, Argentina⁶ Instituto de Astrofísica de La Plata (CCT La Plata—CONICET/UNLP), B1900FWA La Plata, Argentina

Received 2022 September 19; revised 2023 January 19; accepted 2023 January 20; published 2023 February 15

Abstract

WX Cen is most likely one of the Galactic counterparts of compact binary supersoft X-ray sources as a member of the V Sagittae class, in which mass is transferred from a donor secondary to a massive white dwarf primary via an accretion disk. Based on the photometric observations from the TESS space telescope and AAVSO database, 218 times of light minimum were determined. By collecting all available eclipse timings of WX Cen from the literature together with those newly determined, we constructed an $O-C$ diagram and analyzed the variations in the orbital period of the eclipsing binary. It is confirmed that the orbital period is continuously decreasing and the rate of the change in the orbital period is revised to $\dot{P} = -4.4(4) \times 10^{-7} \text{ day yr}^{-1} = -0.038(3) \text{ s yr}^{-1}$. The mass of the donor secondary is estimated as $M_s \sim 0.6 M_\odot$, when the white dwarf mass is $M_{\text{WD}} \sim 0.9 M_\odot$. By considering a conservative mass transfer from the secondary to the primary, the orbital period of WX Cen should be increasing, which is opposite to the observed continuous decrease. Therefore, the decrease in the period can be plausibly explained as the result of angular momentum loss (AML) via magnetic wind from the secondary and/or from the accretion disk. The AML causes the donor secondary with a low mass to continually be filling its critical Roche lobe and transferring material to the white dwarf. In this way, the evolution of WX Cen is dominated by the magnetic wind and continuously radiating supersoft X-rays.

Unified Astronomy Thesaurus concepts: Close binary stars (254); Eclipsing binary stars (444); Orbital evolution (1178)

1. Introduction

WX Cen is located in a high interstellar absorption region near the *Coalsack* at the Galactic plane (Georgelin & Georgelin 1970; Weaver 1974). Nevertheless, it is also a bright object, $V = 13.6\text{--}14.2$ (Diaz & Steiner 1995). Oliveira & Steiner (2004) estimated the color excess of WX Cen as $E(B - V) = 0.63$, and derived a distance of 2.8 ± 0.3 kpc according to the distance–color excess relation. They also determined the intrinsic color of WX Cen as $(B - V)_0 = -0.2$ and the absolute magnitude as $M_V = -0.5$. Moreover, Oliveira & Steiner (2004) confirmed the orbital period of WX Cen determined by Diaz & Steiner (1995) and refined its value to $P_{\text{orb}} = 0.4169615(\pm 22)$ day.

To date, there have been many different opinions regarding the classification of WX Cen. WX Cen was initially resolved by Eggen et al. (1968) as a possible optical counterpart of the hard X-ray transient source Cen XR-2. According to its spectral characteristics, WX Cen was then classified as a Wolf–Rayet star of type WN 7 (Van Der Hucht et al. 1981). However, Vogt (1989) classified WX Cen as a nova-like variable, and then Diaz & Steiner (1995) identified it as the second member of the V Sagittae class of close binary systems. Patterson et al. (1998) also considered the hypothesis of Galactic compact binary supersoft X-ray sources (CBSS) of the stars V Sge, T Pyx, and WX Cen, based on their spectroscopic and photometric properties. Shara et al. (1999) rediscovered WX Cen as a

new WN 3 and named it WR 48c. Nonetheless, the classification of WX Cen is as yet inconclusive.

However, the spectroscopic and photometric characteristics of WX Cen imply that it is most likely one of the Galactic counterparts of CBSS as a member of the V Sagittae class. The light curve of WX Cen has a V-shaped narrow minimum, similar to the ones seen in V Sge stars and CBSS (Oliveira & Steiner 2004). On the other hand, the spectra of WX Cen present highly variable absorption features in the Balmer lines with $V = -2900 \text{ km s}^{-1}$ and in emission with $V = \pm 3500 \text{ km s}^{-1}$, and resemble the satellite emission lines found in the spectra of CBSS (Oliveira & Steiner 2004). Moreover, some highly ionized species are shown in the spectrum observed by Diaz & Steiner (1995), and the He II $\lambda 4686 \text{ \AA}$ line is much stronger than H β ($4686/\text{H}\beta = 2.8$). Such a high $4686/\text{H}\beta$ flux ratio is extremely unusual in cataclysmic variables (CVs), but may be seen in some supersoft sources though with smaller equivalent widths (e.g., CAL 83 and CAL 87, Smale et al. 1988; Cowley et al. 1990; Williams et al. 1991, 1994).

Furthermore, Diaz & Steiner (1995) speculated that there is a semi-opaque stellar wind that is possibly overabundant in helium, according to the Doppler tomograms of Balmer and He II $\lambda 4686 \text{ \AA}$ lines. And the evidence of helium overabundance appears to match the model of nuclear burning on the surface of a white dwarf (Patterson et al. 1998). There is also the double-peaked emission lines from accretion disks in the spectrum of WX Cen observed by Diaz & Steiner (1995). The asymmetric structure in the He II map may be produced in a stream from the secondary and/or in a wind-stream collision (Diaz & Steiner 1995). Moreover, Oliveira & Steiner (2004)

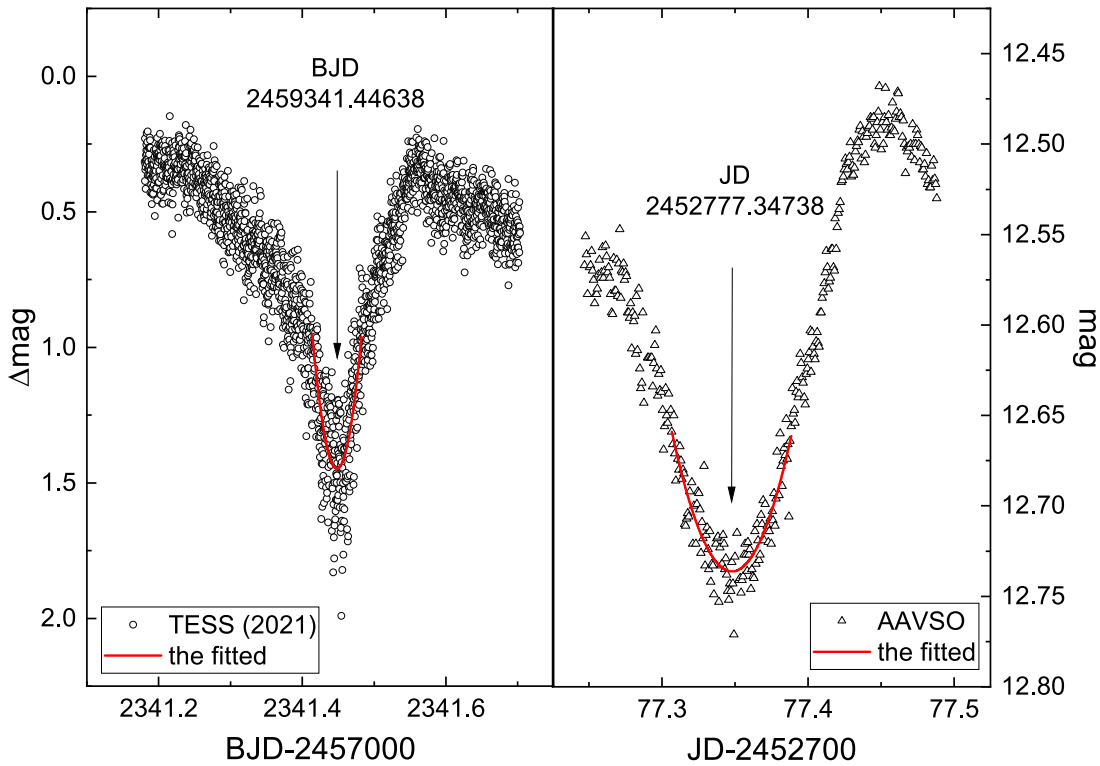


Figure 1. An example of fitting the eclipse timings for WX Cen using the TESS and AAVSO data, respectively.

found that the emission lines of He II $\lambda 4686 \text{ \AA}$ became weaker, which is possibly a sign that WX Cen is tending toward a quiescent phase. However, the X-ray observations of WX Cen and V Sge suggest that their intrinsic X-ray luminosity is below $10^{33} \text{ erg s}^{-1}$. One could interpret such behavior as the absorption of almost all the X-ray flux in WX Cen and V Sge by a geometrically thick disk (Diaz & Steiner 1995).

Therefore, more continuous monitoring at multiple wavelengths is needed to further confirm the classification of WX Cen. In this paper, WX Cen is considered as a Galactic counterpart of CBSS, just like V Sge stars. The origin of the luminosity of CBSS seems to be related to stable nuclear burning of hydrogen accreted onto a white dwarf (van den Heuvel et al. 1992). A high accretion rate ($\sim 10^{-7} M_{\odot} \text{ yr}^{-1}$) is required to produce this process. Two physical mechanisms have been proposed for such an event to occur. Both models imply the presence of strong winds from the irradiated side of the companion and the disk (van den Heuvel et al. 1992; van Teeseling & King 1998). One is that the mass accretion of the white dwarf is supplied through strong winds from the irradiated side of the companion (van Teeseling & King 1998). On the other hand, while the secondary is filling the critical Roche lobe, material is being transferred to the white dwarf on a thermal timescale by Roche-lobe overflow (van den Heuvel et al. 1992). WX Cen is a supersoft X-ray source with a low-mass companion ($M_2/M_1 \lesssim 0.7$), so the mass transfer should cause the orbital period to increase. In the present paper, 218 eclipse times were determined based on photometric data from the Transiting Exoplanet Survey Satellite (TESS) and American Association of Variable Star Observers (AAVSO) databases. We show that the orbital period is continuously decreasing and propose that the decrease in the period is caused by the angular momentum loss (AML) via magnetic wind. Then, the evolutionary process of WX Cen will be discussed.

2. Data Collection

The photometric observations used in this work were obtained with the TESS space telescope and collected by the AAVSO⁷ database. The times of minimum light were determined by fitting the TESS and AAVSO light curves, as well as collected from articles, which are available as supplementary online material.⁸ Like the two instances in Figure 1, 218 newly determined eclipse timings in this work were completed by fitting the TESS and AAVSO light curves using the least-squares method and are tabulated in Table 1.

TESS is a high-precision all-sky photometry survey in space. TESS was launched with the scientific objective of finding extrasolar planets, including those that could support life (Ricker et al. 2014). But in addition, TESS can also accurately detect the more continuous and specific optical variations of stars, which is difficult to achieve with ground-based telescopes. WX Cen is listed in the TESS input catalog (TIC) as TIC 44270808, and was observed in Sector 11 (2019/04/23-2019/05/20) and Sector 38 (2021/04/29-2021/05/26).

These photometric data sets of WX Cen were obtained from the Mikulski Archive for Space Telescopes (MAST⁹) web service. Among them, the light curves observed in 2019 belong to TESS High Level Science Products produced by the MIT Quick-Look Pipeline team (Huang et al. 2020a, 2020b; Kunimoto et al. 2021), from which the normalized simple aperture photometry light curve detrended by Kepler spline (KSPSAP) was extracted to analyze. The light curves observed in 2021 are processed by the Science Processing Operations Center, from which the 20 s cadence data was chosen, and then

⁷ <https://www.aavso.org/databases>

⁸ <https://github.com/zl7788/WXCen>

⁹ <https://mast.stsci.edu/portal/Mashup/Clients/Mast/Portal.html>

Table 1
218 Newly Determined Eclipse Timings for WX Cen Using TESS and AAVSO Data in This Study

Eclipse Timings (BJD-2400000)	Errors (d)	E	$O-C$ (d)	Eclipse Timings (BJD-2400000)	Errors (d)	E	$O-C$ (d)	Eclipse Timings (BJD-2400000)	Errors (d)	E	$O-C$ (d)
52726.47568	0.00040	2559	-0.00442	58603.86437*	0.00094	16655	-0.07008	59331.84962	0.00130	18401	-0.09527
52731.47344	0.00056	2571	-0.01016	58604.27516*	0.00437	16656	-0.07625	59333.93994*	0.00057	18406	-0.08975
52733.56399	0.00047	2576	-0.00442	58604.69747*	0.00156	16657	-0.07089	59334.36074*	0.00054	18407	-0.08591
52734.38320	0.00066	2578	-0.01913	58605.10830*	0.00472	16658	-0.07702	59334.76478*	0.00068	18408	-0.09883
52736.47986	0.00048	2583	-0.00726	58605.52522*	0.00134	16659	-0.07706	59334.77045	0.00150	18408	-0.09316
52737.30801	0.00065	2585	-0.01303	58605.94115*	0.00256	16660	-0.07809	59335.18613*	0.00053	18409	-0.09444
52776.53325	0.00051	2679	0.01806	58606.35675*	0.00264	16661	-0.07945	59335.60383*	0.00059	18410	-0.09370
52777.35186	0.00045	2681	0.00276	58606.78248*	0.00144	16662	-0.07068	59336.02249*	0.00057	18411	-0.09200
52781.50896	0.00074	2691	-0.00973	58607.20381*	0.00268	16663	-0.06631	59336.42799*	0.00074	18412	-0.10345
53803.45573	0.00050	5142	-0.02952	58607.60173*	0.00498	16664	-0.08535	59336.84969*	0.00055	18413	-0.09871
53810.55981	0.00060	5159	-0.01374	58608.02567*	0.00243	16665	-0.07837	59336.85491	0.00137	18413	-0.09350
53831.42421	0.00059	5209	0.00271	58608.44116*	0.00251	16666	-0.07984	59337.27322*	0.00055	18414	-0.09214
53838.49689	0.00032	5226	-0.01292	58608.83858*	0.01004	16667	-0.09937	59337.68503*	0.00059	18415	-0.09729
54599.42851	0.00043	7051	-0.03151	58609.26840*	0.00248	16668	-0.08651	59337.69110	0.00113	18415	-0.09123
54600.28630	0.00085	7053	-0.00763	58614.70541*	0.00246	16681	-0.06997	59338.10154*	0.00046	18416	-0.09774
54601.52685	0.00072	7056	-0.01797	58615.11181*	0.00335	16682	-0.08053	59338.52596*	0.00063	18417	-0.09028
55323.27341	0.00033	8787	-0.02747	58615.53782*	0.00148	16683	-0.07148	59338.94840*	0.00051	18418	-0.08480
56372.74689	0.00099	11304	-0.03984	58615.93866*	0.00332	16684	-0.08760	59339.36579*	0.00062	18419	-0.08437
56375.67530	0.00118	11311	-0.03014	58616.35198*	0.00485	16685	-0.09124	59339.76566*	0.00050	18420	-0.10146
56377.75024	0.00230	11316	-0.04000	58616.77665*	0.00234	16686	-0.08353	59340.20733*	0.00054	18421	-0.07675
56378.59342	0.00155	11318	-0.03073	58617.18175*	0.00222	16687	-0.09538	59340.59823*	0.00045	18422	-0.10280
56380.67249	0.00130	11323	-0.03646	58617.61835*	0.00282	16688	-0.07574	59341.02299*	0.00083	18423	-0.09500
56382.76112	0.00182	11328	-0.03263	58617.62642	0.00152	16688	-0.06768	59341.44638*	0.00047	18424	-0.08857
56383.58551	0.00143	11330	-0.04215	58618.03220*	0.00110	16689	-0.07885	59341.86108*	0.00064	18425	-0.09083
56393.61405	0.00113	11354	-0.02064	58618.45674*	0.00139	16690	-0.07127	59342.28097*	0.00070	18426	-0.08790
56395.68332	0.00070	11359	-0.03616	58618.84563*	0.00301	16691	-0.09934	59342.68705*	0.00093	18427	-0.09878
56400.68867	0.00109	11371	-0.03432	58619.25659*	0.00511	16692	-0.10534	59343.11351*	0.00049	18428	-0.08928
56403.60338	0.00045	11378	-0.03832	58619.69011*	0.00214	16693	-0.08878	59343.51857*	0.00037	18429	-0.10118
56405.69521	0.00150	11383	-0.03128	58619.69413	0.00184	16693	-0.08475	59343.95171*	0.00055	18430	-0.08500
56408.60251	0.00105	11390	-0.04270	58620.11071*	0.00145	16694	-0.08514	59344.36352*	0.00058	18431	-0.09015
56410.70870	0.00138	11395	-0.02130	58620.51920*	0.00540	16695	-0.09361	59344.78295*	0.00049	18432	-0.08767
56411.53442	0.00130	11397	-0.02950	58620.52733	0.00069	16695	-0.08548	59345.20542*	0.00076	18433	-0.08216
56413.61093	0.00072	11402	-0.03778	58620.95766*	0.00182	16696	-0.07211	59345.62126*	0.00112	18434	-0.08328
56418.62275	0.00096	11414	-0.02948	58621.35560*	0.00981	16697	-0.09112	59346.02434*	0.00055	18435	-0.09716
56421.53332	0.00127	11421	-0.03761	58621.78333*	0.00340	16698	-0.08035	59347.69082*	0.00093	18439	-0.09852
56423.61249	0.00095	11426	-0.04324	58622.18765*	0.00154	16699	-0.09299	59348.11912*	0.00090	18440	-0.08718
56441.54587	0.00223	11469	-0.03909	58622.61409*	0.00179	16700	-0.08351	59348.53378*	0.00068	18441	-0.08948
56446.55765	0.00120	11481	-0.03083	58623.04329*	0.00221	16701	-0.07127	59348.94483*	0.00074	18442	-0.09538
56476.57308	0.00082	11553	-0.03644	58623.45699*	0.00243	16702	-0.07453	59349.36014*	0.00061	18443	-0.09703
56484.50135	0.00111	11572	-0.03040	58624.71592	0.00096	16705	-0.06648	59349.79287*	0.00086	18444	-0.08126
57507.69834	0.00228	14026	-0.05084	58627.61661	0.00102	16712	-0.08451	59350.19258*	0.00064	18445	-0.09851
57512.71739	0.00113	14038	-0.03531	58629.70738	0.00180	16717	-0.07852	59350.60715*	0.00047	18446	-0.10090
57525.62325	0.00188	14069	-0.05517	58645.55515	0.00123	16755	-0.07520	59351.02374*	0.00054	18447	-0.10127
57535.62432	0.00113	14093	-0.06111	58652.62657	0.00127	16772	-0.09208	59351.44171*	0.00054	18448	-0.10026
57902.11690	0.00175	14972	-0.07552	58655.56078	0.00055	16779	-0.07658	59351.86889*	0.00054	18449	-0.09004
57902.95969	0.00077	14974	-0.06664	58675.56865	0.00092	16827	-0.08274	59352.28167*	0.00052	18450	-0.09422
57905.03615	0.00103	14979	-0.07498	58680.57268	0.00186	16839	-0.08223	59352.69713*	0.00053	18451	-0.09572
57905.88153	0.00120	14981	-0.06352	58683.49886	0.00193	16846	-0.07476	59353.12307*	0.00047	18452	-0.08674
57907.95308	0.00045	14986	-0.07677	58968.27059	0.00135	17529	-0.08604	59353.51919*	0.00045	18453	-0.10757
58568.83478	0.00131	16571	-0.07511	58972.41804	0.00042	17539	-0.10818	59353.96126*	0.00060	18454	-0.08246
58569.25391	0.00069	16572	-0.07294	58975.35424	0.00051	17546	-0.09069	59354.35740*	0.00064	18455	-0.10328
58569.68294	0.00129	16573	-0.06087	58978.28403	0.00038	17553	-0.07962	59354.79141*	0.00054	18456	-0.08623
58570.08265	0.00068	16574	-0.07812	58980.36372	0.00041	17558	-0.08472	59355.20179*	0.00053	18457	-0.09281
58573.00435	0.00085	16581	-0.07513	58981.62424	0.00132	17561	-0.07508	59355.60694*	0.00051	18458	-0.10462
58575.08855	0.00081	16586	-0.07573	58983.29266	0.00053	17565	-0.07449	59356.04123*	0.00059	18459	-0.08729
58586.75818	0.00090	16614	-0.08095	58989.52216	0.00149	17580	-0.09938	59356.45921*	0.00062	18460	-0.08627
58587.59403	0.00179	16616	-0.07901	58991.63591	0.00085	17585	-0.07042	59356.86908*	0.00058	18461	-0.09336
58588.85147	0.00103	16619	-0.07245	58994.54739	0.00055	17592	-0.07766	59357.27759*	0.00052	18462	-0.10181
58591.76244	0.00120	16626	-0.08019	58996.62683	0.00088	17597	-0.08301	59357.70185*	0.00063	18463	-0.09450
58592.59439	0.00151	16628	-0.08216	58999.53519	0.00119	17604	-0.09337	59357.70222	0.00061	18463	-0.09413
58593.84878	0.00141	16631	-0.07865	59004.54776	0.00111	17616	-0.08431	59358.12041*	0.00060	18464	-0.09290
58596.77011	0.00164	16638	-0.07603	59014.55353	0.00137	17640	-0.08555	59358.51675*	0.00066	18465	-0.11352
58597.58822	0.00116	16640	-0.09184	59019.56114	0.00151	17652	-0.08145	59358.95439*	0.00067	18466	-0.09284

Table 1
(Continued)

Eclipse Timings (BJD-2400000)	Errors (d)	E	$O-C$ (d)	Eclipse Timings (BJD-2400000)	Errors (d)	E	$O-C$ (d)	Eclipse Timings (BJD-2400000)	Errors (d)	E	$O-C$ (d)
58598.85306	0.00235	16643	-0.07788	59276.82863	0.00195	18269	-0.07767	59359.38831*	0.00051	18467	-0.07588
58599.68826	0.00055	16645	-0.07660	59296.82777	0.00089	18317	-0.09257	59359.78370*	0.00065	18468	-0.09745
58600.51201*	0.02258	16647	-0.08676	59299.74337	0.00233	18324	-0.09568	59360.20577*	0.00050	18469	-0.09234
58600.91861*	0.00694	16648	-0.09712	59301.84397	0.00144	18329	-0.07987	59365.61619	0.00146	18482	-0.10239
58601.36043*	0.00295	16649	-0.07226	59304.76596	0.00180	18336	-0.07660	59366.48141	0.00120	18484	-0.07108
58601.77474*	0.00174	16650	-0.07491	59306.84660	0.00104	18341	-0.08076	59385.63757	0.00191	18530	-0.09504
58602.17186*	0.00951	16651	-0.09475	59307.67358	0.00093	18343	-0.08769	59393.56924	0.00052	18549	-0.08559
58602.59693*	0.00277	16652	-0.08664	59325.60010	0.00213	18386	-0.09041	59396.49167	0.00351	18556	-0.08188
58602.98082*	0.00569	16653	-0.11971	59327.68145	0.00103	18391	-0.09386	59413.58075	0.00109	18597	-0.08811
58603.41184*	0.00432	16654	-0.10565	59329.76014	0.00087	18396	-0.09996				

Note. The eclipse timings with an asterisk are obtained from TESS data.

the Pre-search Data Conditioning Simple Aperture Photometry flux was extracted to use in our analysis.

3. Analysis of the Change in the Orbital Period

The changes in the orbital period of WX Cen were analyzed by using times of minimum light determined from the TESS and AAVSO light curves and those published in Oliveira & Steiner (2004) and Qian et al. (2013). For WX Cen, epochs and $O-C$ values were calculated for the available eclipse times according to the linear component of the ephemeris from Qian et al. (2013):

$$\text{Min}.I = \text{HJD}2451659.4812 + 0.41695902E. \quad (1)$$

As displayed in Figure 2, all $O-C$ values can be fitted by a parabola model function (shown with the solid line) using the least-squares method, which represents the calculated quadratic ephemeris

$$\text{Min}.I = \text{BJD}2451659.481(2) + 0.4169587(4)E - 2.5(2) \times 10^{-10}E^2. \quad (2)$$

Analysis of variance (i.e., F-test) was used to estimate the confidence level of this fit. The result indicates that the quadratic term is significant at more than the 99.99% level. The errors of fitted parameters are the unbiased standard errors (covering the 68% confidence interval). The dashed line represents the quadratic ephemeris calculated by Qian et al. (2013).

The orbital period of WX Cen has previously been revised by Oliveira & Steiner (2004), and then a long-term decrease in the orbital period has been proposed by Qian et al. (2013). In this work, the $O-C$ diagram still shows a downward parabolic variation, which clearly illustrates that the orbital period is decreasing. According to the quadratic term in Equation (2), the period is decreasing at a rate of

$$\dot{P} = -1.2(1) \times 10^{-9} \text{ s s}^{-1} = -4.4(4) \times 10^{-7} \text{ day yr}^{-1}, \quad (3)$$

while the latest value is $-5.15 \times 10^{-7} \text{ day yr}^{-1}$ determined by Qian et al. (2013) up to now. The error propagation formula was used to estimate the standard errors for the derived parameters. This discrepancy between previous values and our value is most likely due to differences in the number of eclipse times and time spans.

4. Discussions and Conclusions

4.1. Estimate of the Component Masses of WX Cen

For WX Cen, the determination of the nature and mass of its components is still unresolved and extremely important. Diaz & Steiner (1995) present a detailed discussion on this issue. The authors argue that (1) if the mass of the Roche-lobe filling ZAMS secondary is $M_2 \simeq 1.16 M_\odot$, then the primary has a mass $M_1 \geq 3.5(\pm 0.5) M_\odot$; (2) if the primary is a white dwarf with a limit mass of $M_1 = 1.4 M_\odot$, then the secondary should have a mass $M_2 = 0.35 M_\odot$; (3) Perhaps there is a nondegenerate high mass primary in WX Cen, such as a helium main-sequence star, but the possibility of a neutron or even a black hole primary is unlikely.

However, Oliveira & Steiner (2004) speculated that the intrinsic velocity of the *jet* as $V = 6100 \text{ km s}^{-1}$ according to the satellite-like events at the Balmer lines, which corresponds to the escape velocity of a white dwarf with a mass of $M \sim 0.9 M_\odot$. In addition, by comparing the light curve of WX Cen with that of QR And, Oliveira & Steiner (2004) adopted the same inclination as QR And for WX Cen, which is $i = 55^\circ$. In this work, similar to the measurement of the radial-velocity semi-amplitude of the white dwarf (K_{WD}) in U Sco by Thoroughgood et al. (2001), the He II $\lambda 4686 \text{ \AA}$ line was considered as a reliable representation of the motion of the white dwarf. Thus, the white dwarf radial-velocity semi-amplitude of WX Cen is $K_{\text{WD}} = 108 \pm 3 \text{ km s}^{-1}$ (Diaz & Steiner 1995; Oliveira & Steiner 2004). But the radial velocity of the secondary is unknown because no absorption features from the secondary could be found in the optical spectrum of WX Cen (Diaz & Steiner 1995).

Combined with the above information, the relation between the masses of two components is derived, as displayed in Figure 3, using Equation (8) in Pyrzas et al. (2009)

$$\frac{(M_s \sin i)^3}{(M_{\text{WD}} + M_s)^2} = \frac{P_{\text{orb}} K_{\text{WD}}^3}{2\pi G}. \quad (4)$$

The inclination is assumed as $i = 50^\circ$, $i = 55^\circ$, and $i = 60^\circ$ respectively. The filled area denotes the K_{WD} offset of $\pm 3 \text{ km s}^{-1}$ and centering on 108 km s^{-1} . As shown in Figure 3, when the white dwarf mass is $M_{\text{WD}} \sim 0.9 M_\odot$, the secondary has a mass of $M_s \sim 0.6 M_\odot$.

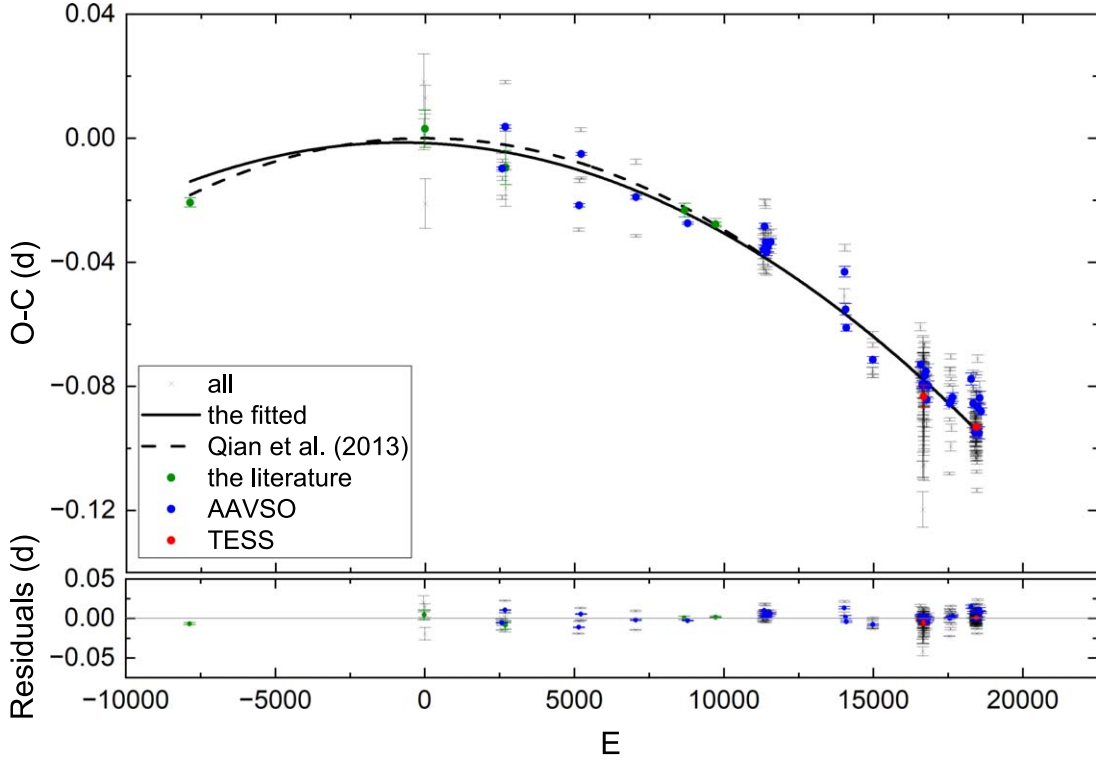


Figure 2. The $O-C$ diagram for WX Cen (using an orbital period of 0.41695902 day from the ephemeris of Qian et al. 2013). All the $O-C$ values were used for the fit. The binned (at intervals of 30 cycles) and averaged $O-C$ (color points) values are also displayed in this figure for aesthetic reasons, in which the TESS data observed in the same sector was averaged to be one point due to continuity.

4.2. AML Driven by Magnetic Wind

Qian et al. (2013) reported the discovery of the decreasing orbital period of WX Cen for the first time. The authors interpreted such behavior as there being a more massive donor secondary than the white dwarf in CBSS WX Cen, which transfers mass to the white dwarf by thermal-timescale Roche-lobe overflow. However, in this paper, an alternative explanation is proposed, in which the AML causes the orbit to shrink, which is driven by the magnetic wind from the secondary and/or from the accretion disk. Meanwhile, due to the continuous contraction of the orbit, the donor secondary with a low mass can always be filling its critical Roche lobe and transferring material to the white dwarf.

In the above evolutionary scenario, the change in the total angular momentum is primarily comprised of that of intrinsic orbital angular momentum and AML driven by the magnetic wind, which is proposed by Tout & Hall (1991) as

$$\dot{J} = \dot{M}d_1^2\Omega + KJ. \quad (5)$$

\dot{M} is the rate of total mass loss from the system, d_1 is the distance of the donor from the center of mass, Ω is the angular velocity about the center of mass ($\Omega = 2\pi/P$, where P is the orbital period) and KJ represents AML driven by the magnetic wind in this work. The corresponding orbital period change is given by Tout & Hall (1991), that is,

$$\frac{\dot{P}}{P} = -\frac{2\dot{M}}{M} + \frac{3\dot{M}_2(M_2 - M_1)}{M_1M_2} + 3K, \quad (6)$$

where

$$K = \frac{2}{3} \left(\frac{R_A}{d} \right)^2 \frac{M}{M_1M_2} \dot{M}. \quad (7)$$

For WX Cen, M_1 is the mass of the white dwarf, M_2 is the mass of the donor secondary, $M = M_1 + M_2$ is the total mass, R_A is Alfvén radius, and d is the binary separation.

The mass-loss rate of the donor secondary is $\dot{M}_2 = \dot{M}_{2w} + \dot{M}_{2tr}$. \dot{M}_{2w} is the rate of the secondary’s wind mass loss and \dot{M}_{2tr} denotes the mass-transfer rate. The model for enhanced stellar wind mass loss is proposed by Tout & Eggleton (1988),

$$\dot{M}_{2w} = -4 \times 10^{-13} \frac{R_2 L_2}{M_2} \left\{ 1 + 10^4 \left(\frac{R_2}{R_L} \right)^6 \right\} (M_\odot \text{ yr}^{-1}), \quad (8)$$

with R_2 , L_2 and M_2 in solar units. R_2 , L_2 , and R_L is the radius, the luminosity and the Roche-lobe radius of the donor secondary, respectively. Based on Kepler’s third law for a circular orbit, using $M_1 = 0.9 M_\odot$, $M_2 = 0.6 M_\odot$ and $P = 0.416959$ day, $d = 2.7 R_\odot$ is derived. Then using the dependence of R_L/d on the mass ratio q ($q = \frac{M_2}{M_1}$),

$$\frac{R_L}{d} = \frac{0.49q^{\frac{2}{3}}}{0.6q^{\frac{2}{3}} + \ln(1 + q^{\frac{1}{3}})}, \quad (9)$$

found by Eggleton (1983), considering a Roche-filling star ($R_2 = R_L$), $R_2 = 0.93 R_\odot$ is derived. According to the formula $L_2 = 4\pi R_2^2 \sigma T_2^4$, where the effective temperature of the donor secondary $T_2 \sim 5782 K$ obtained from Gaia DR3

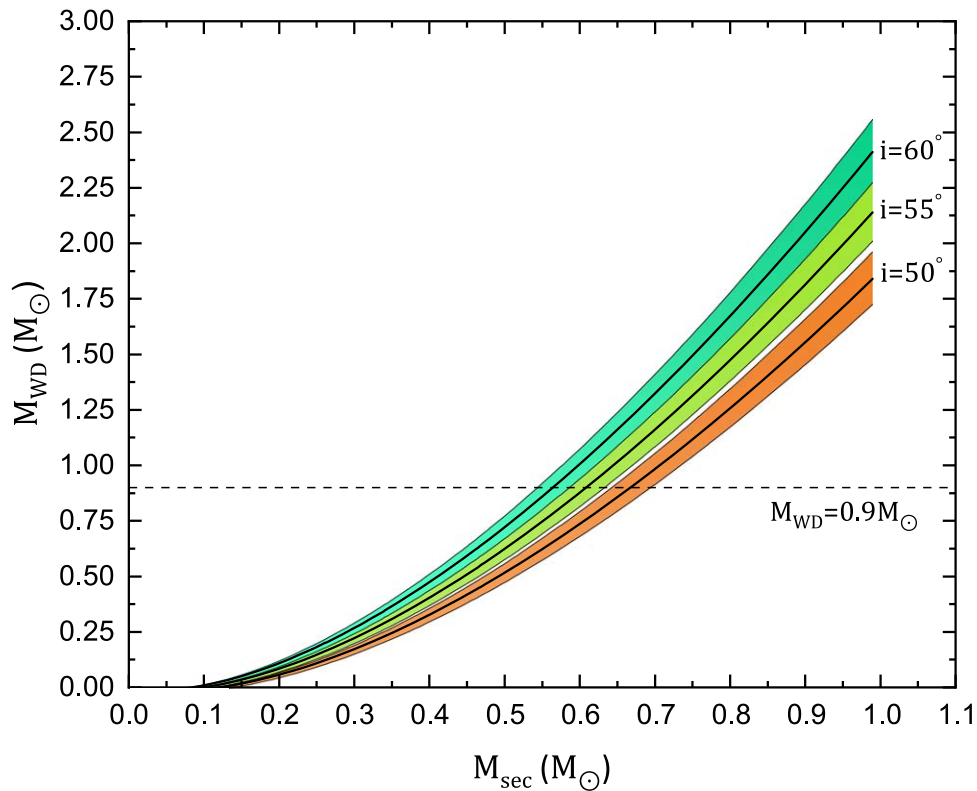


Figure 3. The relation between the masses of two components. The inclination is assumed as $i = 50^\circ$, $i = 55^\circ$, and $i = 60^\circ$ respectively. The filled area denotes the K_{WD} offset of $\pm 3 \text{ km s}^{-1}$ and centering on 108 km s^{-1} . When the white dwarf mass is $M_{\text{WD}} \sim 0.9 M_\odot$, the secondary has a mass of $M_s \sim 0.6 M_\odot$.

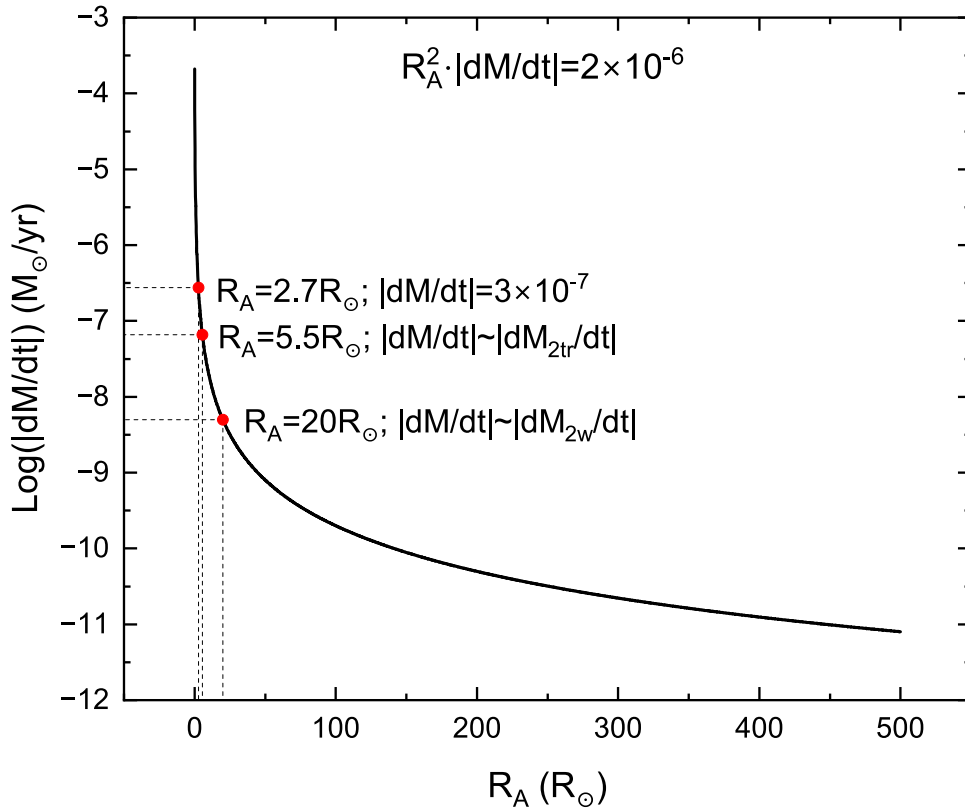


Figure 4. The relation between the mass-loss rate (\dot{M}) and the Alfvén radius (R_A). See the text for details.

(Gaia Collaboration 2022), $L_2 = 0.87L_\odot$ is computed. Consequently, the mass-loss rate of the stellar wind for the donor secondary is derived as $\dot{M}_{2w} \simeq -5 \times 10^{-9} M_\odot \text{ yr}^{-1}$. It is assumed that the donor secondary transfers matter on the thermal timescale, that is $\tau_{M_2} = \frac{M_2}{|\dot{M}_{2tr}|} \simeq \tau_{\text{KH}}$. Applying the formula of the Kelvin–Helmholtz timescale

$$\tau_{\text{KH}} = 2 \times 10^7 \frac{M_2^2}{R_2 L_2}, \quad (10)$$

the mass-transfer rate is calculated to be $\dot{M}_{2tr} \simeq -6.7 \times 10^{-8} M_\odot \text{ yr}^{-1}$.

In general, a substantial part of the total mass loss of the system comes from the stellar wind of the donor secondary (the rest may be from the disk wind). Thus, the value of the first term in Equation (6) is about $1 \times 10^{-8} \text{ yr}^{-1}$, which is two orders of magnitude smaller than $\dot{P}/P \sim -1 \times 10^{-6} \text{ yr}^{-1}$, so it is negligible. Consequently, the relation between the total mass-loss rate (\dot{M}) and the Alfvén radius (R_A) is estimated as $R_A^2 \dot{M} = -2 \times 10^{-6} R_\odot^2 M_\odot \text{ yr}^{-1}$ from Equation (6), and is shown in Figure 4. The total magnetic wind mass loss is probably contributed by two mechanisms alone or together: (1) the magnetic stellar wind from the donor secondary; (2) the magnetic disk wind from the accretion disk, similar to the accretion disk wind in V Sge. From the point of view of magnetic stellar wind, if the total mass-loss rate is comparable to that of the stellar wind for the donor secondary, i.e., $\dot{M} \sim -5 \times 10^{-9} M_\odot \text{ yr}^{-1}$, the required Alfvén radius will be about $20 R_\odot$, which is in the range of the solar average Alfvén radius (Goelzer et al. 2014; Liu et al. 2021). However, if the Alfvén radius gets smaller, the mass-loss rate required to reduce the orbital period will be too high to be supported by stellar wind loss alone. On the other hand, the magnetic disk wind can also carry off orbital angular momentum. As computed by Livio & Pringle (1994), its Alfvén radius is equal to the binary separation at least (i.e., $R_A = 2.7 R_\odot$ for WX Cen), then the required mass-loss rate is up to $\dot{M} = -3 \times 10^{-7} M_\odot \text{ yr}^{-1}$, which is larger than the mass-transfer rate. By considering that the total mass-loss rate is comparable to that of the mass transfer (i.e., $\dot{M} \sim \dot{M}_{2tr}$), the required Alfvén radius is about $5.5 R_\odot$. In this case, although secondary magnetic braking can take effect, it does so only at a low level (Livio & Pringle 1994).

5. Summary

In this work, by using TESS and AAVSO data, we determined 218 new times of light minimum for the CBSS WX Cen. The orbital period variation of WX Cen has been analyzed and the latest rate of orbital period decrease $\dot{P} = -1.2(1) \times 10^{-9} \text{ s s}^{-1}$ was calculated. The mass of the donor secondary is estimated as $M_s \sim 0.6 M_\odot$, when the white dwarf mass is $M_{\text{WD}} \sim 0.9 M_\odot$. By considering a conservative mass transfer from the secondary to the primary, the orbital period of WX Cen should be increasing, which is opposite to the observed continuous decrease. To interpret such behavior, it was proposed that the continuously decreasing orbital period may be dominated by the AML, which is driven by the magnetic wind from the secondary and/or from the accretion disk. Since the orbit is shrinking, it was assumed that the donor secondary with a low mass can always be filling its critical Roche lobe and transferring material to the white dwarf. The relation between the total mass-loss rate (\dot{M}) and the Alfvén radius (R_A) was estimated as $R_A^2 \dot{M} = -2 \times 10^{-6} R_\odot^2 M_\odot \text{ yr}^{-1}$ in

this evolutionary scenario. More continuous monitoring at multiple wavelengths is needed to further confirm the nature and masses of components of WX Cen.

This work is supported by the National Natural Science Foundation of China (Nos. 11933008 and 11873017) and the basic research project of Yunnan Province (grant No. 202201AT070092). We acknowledge with sincerest thanks the released observations from TESS. The TESS data presented in this paper were obtained from the Mikulski Archive for Space Telescopes (MAST) at the Space Telescope Science Institute (STScI). STScI is operated by the Association of Universities for Research in Astronomy, Inc. Support to MAST for these data is provided by the NASA Office of Space Science. Funding for the TESS mission is provided by the NASA Explorer Program. We thank the variable star observations from the AAVSO International Database contributed by observers worldwide and used in this research.

Facilities: TESS, MAST, AAVSO.

Data Availability

The photometric data analyzed in this article were accessed from MAST and AAVSO, <https://mast.stsci.edu/portal/Mashup/Clients/Mast/Portal.html> and <https://www.aavso.org/databases>. All the eclipse times generated and analyzed in this article were stored at <https://github.com/zl7788/WXCen>.

ORCID iDs

Lei Zang  <https://orcid.org/0000-0003-1674-0890>

References

- Cowley, A. P., Schmidtke, P. C., Crampton, D., & Hutchings, J. B. 1990, *ApJ*, **350**, 288
- Diaz, M. P., & Steiner, J. E. 1995, *AJ*, **110**, 1816
- Eggen, O. J., Freeman, K. C., & Sandage, A. 1968, *ApJL*, **154**, L27
- Eggleton, P. P. 1983, *ApJ*, **268**, 368
- Gaia Collaboration 2022, VizieR Online Data Catalog I/355, Gaia Data Release 3 (Gaia DR3) Part 1 Main source
- Georgelin, Y. P., & Georgelin, Y. M. 1970, *A&AS*, **3**, 1
- Goelzer, M. L., Schwadron, N. A., & Smith, C. W. 2014, *JGRA*, **119**, 115
- Huang, C. X., Vanderburg, A., Pál, A., et al. 2020a, *RNAAS*, **4**, 204
- Huang, C. X., Vanderburg, A., Pál, A., et al. 2020b, *RNAAS*, **4**, 206
- Kunimoto, M., Huang, C., Tey, E., et al. 2021, *RNAAS*, **5**, 234
- Liu, Y. D., Chen, C., Stevens, M. L., & Liu, M. 2021, *ApJL*, **908**, L41
- Livio, M., & Pringle, J. E. 1994, *ApJ*, **427**, 956
- Oliveira, A. S., & Steiner, J. E. 2004, *MNRAS*, **351**, 685
- Patterson, J., Kemp, J., Sharnbrook, A., et al. 1998, *PASP*, **110**, 380
- Pyrzas, S., Gansicke, B. T., Marsh, T. R., et al. 2009, *MNRAS*, **394**, 978
- Qian, S. B., Shi, G., Fernández Lajús, E., et al. 2013, *ApJL*, **772**, L18
- Ricker, G. R., Winn, J. N., Vanderspek, R., et al. 2014, *JATIS*, **1**, 1
- Shara, M. M., Moffat, A. F. J., Smith, L. F., et al. 1999, *AJ*, **118**, 390
- Smale, A. P., Corbet, R. H. D., Charles, P. A., et al. 1988, *MNRAS*, **233**, 51
- Thoroughgood, T. D., Dhillon, V. S., Littlefair, S. P., Marsh, T. R., & Smith, D. A. 2001, *MNRAS*, **327**, 1323
- Tout, C. A., & Eggleton, P. P. 1988, *MNRAS*, **231**, 823
- Tout, C. A., & Hall, D. S. 1991, *MNRAS*, **253**, 9
- van den Heuvel, E. P. J., Bhattacharya, D., Nomoto, K., & Rappaport, S. A. 1992, *A&A*, **262**, 97
- Van Der Hucht, K. A., Conti, P. S., Lundstrom, I., & Stenholm, B. 1981, *SSRv*, **28**, 227
- van Teeseling, A., & King, A. R. 1998, *A&A*, **338**, 957
- Vogt, N. 1989, in *Classical Novae*, ed. M. F. Bode & A. Evans (New York: Wiley)
- Weaver, B. W. 1974, *ApJ*, **189**, 263
- Williams, R. E., Hamuy, M., Phillips, M. M., et al. 1991, *ApJ*, **376**, 721
- Williams, R. E., Phillips, M. M., & Hamuy, M. 1994, *ApJS*, **90**, 297